

Journal of Materials Chemistry A

Accepted Manuscript



This is an *Accepted Manuscript*, which has been through the Royal Society of Chemistry peer review process and has been accepted for publication.

Accepted Manuscripts are published online shortly after acceptance, before technical editing, formatting and proof reading. Using this free service, authors can make their results available to the community, in citable form, before we publish the edited article. We will replace this *Accepted Manuscript* with the edited and formatted *Advance Article* as soon as it is available.

You can find more information about *Accepted Manuscripts* in the [Information for Authors](#).

Please note that technical editing may introduce minor changes to the text and/or graphics, which may alter content. The journal's standard [Terms & Conditions](#) and the [Ethical guidelines](#) still apply. In no event shall the Royal Society of Chemistry be held responsible for any errors or omissions in this *Accepted Manuscript* or any consequences arising from the use of any information it contains.

Cite this: DOI: 10.1039/c0xx00000x

www.rsc.org/xxxxxx

ARTICLE TYPE

Stokes shift/emission efficiency trade-off in donor-acceptor perylene monoimides for luminescent solar concentrators.

Riccardo Turrisi,^{a,c} Alessandro Sanguineti,^a Mauro Sassi,^a Brett Savoie,^c Atsuro Takai,^c Giorgio E. Patriarca,^a Matteo M. Salamone,^a Riccardo Ruffo,^a Gianfranco Vaccaro,^a Francesco Meinardi,^a Tobin J. Marks,^c Antonio Facchetti^b and Luca Beverina^{a,*}

Received (in XXX, XXX) Xth XXXXXXXXX 20XX, Accepted Xth XXXXXXXXX 20XX

DOI: 10.1039/b000000x

Perylenediimides (PDIs) are among the most performing organic luminescent materials, both in terms of emission efficiency and chemical and photochemical stability thanks to their rigid, symmetric and planar structure. However, they exhibit very small Stokes shifts. The sizeable reabsorption of the emitted light limits perylenediimides performances for example in imaging applications and luminescent solar concentrators. Perylenemonoimides (PMIs) having an electron donating substituent in one of the free positions feature larger Stokes shift values, while retaining high chemical stability. Selection of the most appropriate donor, both in terms of electron donating capabilities and steric demand, boosts emission efficiency and limits reabsorption losses. The synthesis, optical spectroscopy, molecular orbital computations, UPS, electrochemical, spectroelectrochemical, and multinuclear NMR investigation of a series of PMI derivatives functionalized with donors having different electronic characteristics and steric demands are discussed. Results are relevant for the fabrication of single layer, plastic Luminescent Solar Concentrators (LSC).

Introduction

Perylene dyes are among the most successful π -conjugated organic derivatives for optoelectronic applications. Their most relevant features include flexibility in the chemical structure, tuning of electrical, optical and optoelectronic properties, low toxicity, high absorption and emission efficiencies as well as unrivalled photo, thermo and chemical stability.¹⁻⁵ As such, perylene dyes have found applications in diverse research fields such as organic field effect transistors,⁶⁻¹⁰ dye lasers,¹¹ donor-acceptor dyads,^{12,13} sensors,^{14,15} imaging and bioimaging,¹⁶⁻¹⁸ nonlinearoptics¹⁹⁻²¹ and dye sensitized²²⁻²⁵ and bulk heterojunction solar cells.^{26,27} Perylenediimides (PDIs), under the brand name of Lumogen, are also the core active component of luminescent solar concentrators (LSCs), a class of light concentrating devices introduced in the early '70s and recently revisited in view of their applicability in building integrated photovoltaics.²⁸⁻³¹

The LSC concept was introduced to reduce production costs and overcome some limitations of standard silicon-based photovoltaics without changing the basic photon-to-current conversion technology (silicon single junction cells). Moreover, these devices possess building integration opportunities even greater than those of large area dye sensitized solar cells. In their most common embodiment, LSCs are slabs of transparent, high-quality optical materials doped with luminescent molecules.³² The host material is typically poly(methylmethacrylate)

(PMMA), although in specific cases other materials can be used.^{33,34} The embedded luminescent molecules absorb sunlight and emit light inside the slab. If the refractive index of the slab is significantly higher than that of the air, most of the emitted light is trapped by total internal reflection. The emitted light will travel to the slab edges and there be collected in a small area where a standard silicon solar cell is located. The advantages of such strategy are: 1) The LSC is a light collector where diffuse light over a large area is concentrated at the slab edges; this is useful, since Silicon PV cells need a certain light intensity threshold to convert light into electricity. 2) Strong reduction in the amount of silicon in the cell since it is required only to cover the LSC slab edges. 3) The slabs can be easily integrated with buildings due to wide colour tuning capabilities. If properly engineered, a LSC can be at the same time a structural component (for example in sunroofs and windows), an active energy-producing device and a decorative element.

The main limitation of the LSC concept is the re-absorption of the emitted light due to incomplete spectral separation between the dye absorption and emission spectra.³⁵ This effect strongly limits the slab maximum collecting surface. Recently Currie et al. demonstrated that the use of bi-layer structures consisting of a thin film of organic dyes vacuum deposited on a high-refractive-index glass efficiently reduces re-absorption losses.³⁶ Further optimizations of the LSC structure have also been recently proposed.^{31,37-39} Low cost, plastic, single layer LSCs require the design of efficient luminophores, having complete spectral separation between absorption and emission (i.e. large Stokes

shifts). Moreover, the dye should absorb the largest possible portion of the solar spectrum, efficiently emit in the slab as well as withstand direct exposure to solar light and possibly extreme weather conditions for years. Among various chromophore classes for LSCs (rhodamines²⁸ and coumarines,⁴⁰ oligothiophenes,³³ phycobilisomes,⁴¹ lanthanide chelates⁴²⁻⁴⁷ and more recently quantum dots^{38,48-50}) perylenediimides represent the state-of-the art in LSC materials, even though their Stokes Shift is very small.^{51,52}

Molecules featuring a large Stokes shift pertain to two main classes, having in common a large change in the molecular structure upon optical excitation (Figure S1, Supporting Information): a) donor-acceptor derivatives (D-A) and b) twisted (TW) structures. In D-A derivatives the optical transition involves a redistribution of the electron density from an electron-rich group (the donor) to an electron-poor one (the acceptor), through a conjugated bridge.⁵³⁻⁵⁶ This is by far the broader class of large Stokes shift derivatives, finding applications for example in fluorescence bio-imaging.^{57,58} Efficient D-A fluorophores feature rigid, planar and easily polarizable conjugated bridges enabling for large changes in the electronic distribution upon optical excitation.

Conversely, TW molecules possess conjugated bridges having substantial deviation from planarity. The *p*-terphenyl molecule represents a good example of this class of materials (see Figure S1). Optical excitation involves a transition from the aromatic and twisted ground state structure to a quinoidal excited state structure having formal double bonds connecting the neighboring benzene rings. The resulting major variations in the molecular electronic structure translates into a large Stokes shift.^{59,60} While the PDI core cannot be manipulated to fit in any of two such classes, perylenemonimides (PMIs) can display a rather pronounced D-A character, provided that they carry a strong electron donating substituent in one or both free *peri* positions.^{53,61-66} Also, substitution at the same positions with bulky arenes leads to TW-type structures having relevant Stokes shifts, as demonstrated by the PMI dimers prepared by the Langhals group.⁶⁷

In specific cases, i.e. when the arene introduced at one of the free *peri* positions is bulky and is also a donor group, the resulting PMI will behave according to a combination of the D-A and TW governed regimes. The capability to control the interplay of the TW vs. D-A contributions in PMIs could provides a tool for further optimization of these compounds for LSC applications. In fact, while twisted structures usually feature high fluorescence efficiency and modest molar absorptivity, the opposite occurs for donor-acceptor compounds.

The present paper aims at studying the influence of the donor residue electronic and steric characteristics on the Stokes shift and emission efficiency in a series of PMIs (1-5, Figure 1) for single layer LSC. These derivatives were investigated by steady-state UV-Vis absorption and emission spectroscopies, UV-Vis transient absorption spectroscopy, electrochemistry, spectroelectrochemistry, UPS and multinuclear NMR measurements to establish general structure-properties relationships. We will then show how the molecular properties dominate single layer LSC efficiencies, with particular emphasis on reabsorption losses.

Chromophore's Design and Synthesis.

Figure 1 shows the chemical structure of the PMI derivatives investigated in this study along with that of the planar/rigid derivative **PMI-qs**⁶⁸ used here for comparison. Derivatives **1-5** share the same PMI core and differ for the donor group at the *peri* position. Aiming at establishing structure-property relationships ruling emission efficiency and extent of the Stokes shift, we selected a series of donor groups sharing, except for derivative **1**, the same donating centre, a nitrogen atom featuring an available lone pair, embedded in very diverse electronic structures.

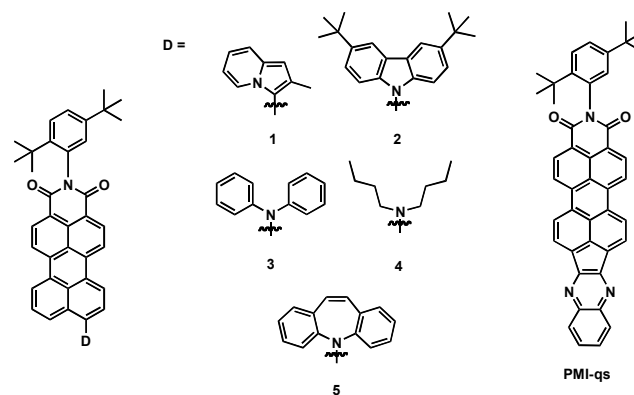


Figure 1.

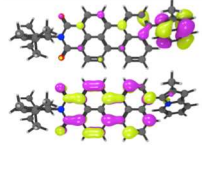
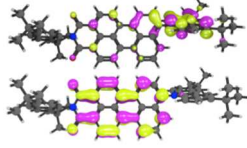
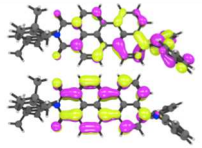
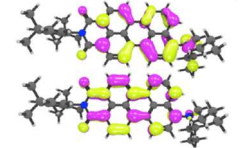
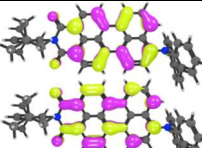
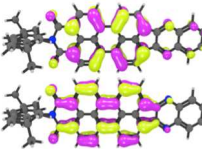
In details, molecule **1** features an indolizine donor where the nitrogen lone pair involved in the substituent π orbital makes the pentatomic ring π -excessive, and thus electron donating. The molecule is connected to the perylene core through its 1-position. This is the only member of this series featuring a carbon-carbon bond between the donor and the perylene core. Molecule **2** possesses a carbazole donor directly connected to the perylene core through the nitrogen atom. Since the central ring of carbazole is aromatic, the nitrogen lone pair, involved in the carbazole π orbital, is not particularly prone to delocalization towards the PMI electron-withdrawing end. Derivatives **3** and **4** have already been described in the literature as D-A molecules.^{53,64,65} In terms of donating capabilities, it can be anticipated that a dialkylamine will be a stronger donor due to the lack of delocalization of the nitrogen lone pair over aryl substituents rather than the perylene core.⁶⁹ Moreover, derivative **4** is the only member of the series that can be described as a purely D-A molecule without TW contribution. Finally, derivative **5** features a dibenzoazepine donor, directly connected with the perylene core through its nitrogen atom. The central ring of dibenzoazepine features 8 π electrons and therefore, as per Hückel's definition, it is antiaromatic. Thus, the nitrogen lone pair should be extremely prone to delocalize, since donation of the electron pair would provide aromatic stabilization. It should be noted that Hückel rule applies for monocyclic, planar compounds. The case of dibenzoazepine is different, and thus deviations from a purely antiaromatic behaviour are expected.⁷⁰ The synthesis of derivatives **1-5** is reported in Scheme S1 of the Supporting Information. The key intermediate for all of the compounds is the unsubstituted perylene monoimide **7**. The latter can be prepared, according to the method of Langhals, by the condensation/decarboxylation reaction of perylendianhydride **6** and 3,5-ditertbutylaniline.⁷¹ This reaction was carried out using

imidazole as the solvent and in the presence of $\text{Zn}(\text{AcO})_2$ in a steel autoclave at 190°C for 24 h. Pure **6** can be isolated in 33% yield after chromatographic purification. Regioselective bromination of **6**, according to Nagao procedure, gives the bromide **8** in 91% yield after chromatographic purification.⁷² Derivative **1** was prepared by direct arylation of 2-methylindolizine with bromide **8**. This type of reactions are becoming relevant due to the lack of toxic/difficult to remove organometallic intermediates and the generally high yields, once the reaction conditions are optimized.⁷³ We obtained the best results working under Fagnou conditions⁷⁴, using DMAc at 100°C with $\text{Pd}(\text{AcO})_2/\text{P}(\text{cyclohexyl})_3\text{HBF}_4$ as the catalyst in the presence of pivalic acid and K_2CO_3 as a base. Different from all other compounds in the series, derivative **1** proved to be air unstable. The Buchwald-Hartwig amination of **8** with 4,7-di-tert-butylcarbazole, diphenylamine, dibutylamine and dibenzoazepine gives derivatives **2** (41%), **3** (70%), **4** (70%) and **5** (75%), respectively. The reaction conditions were the same for all of the compounds: we used a $\text{Pd}(\text{dba})_2/\text{P}(\text{tBu})_3$ catalyst in refluxing toluene with *tert*-BuONa as the base. We carried out these reactions for 6-8 h under microwave irradiation. The conversion was complete in all of the cases while the reaction yields reflected the nucleophilicity of the donor nitranion.

25 Molecular Orbital Computations.

In order to obtain insights into the electronic structure and geometry of the PMI derivatives, particularly molecular planarity upon donor variation, we carried out molecular orbital computations.⁷⁵ All DFT calculations were performed using the Q-Chem software suite, details are discussed in the Supporting Information.⁷⁶ Table 1 shows the calculated ground state geometries, HOMO and LUMO energies, torsional angle between the donor and perylene core and the dipole moments of derivatives **1-5** and of reference molecule **PMI-qs**. Derivatives **1** and **2** featuring the planar and rigid indolizine and carbazole donating groups, respectively, exhibit remarkably large torsional angles with respect to the perylene core (61° and 62° , respectively). MO calculations give a ground state dipole moment higher for derivative **1** (5.93 Debye) than for derivative **2** (4.75 Debye). Derivative **3** having a diphenylamine donating group is also considerably twisted (45°) and shows a calculated dipole moment of 6.70 Debye, which is larger than that of both **1** and **2**. Finally, derivative **5** structure shows that first of all the central ring of the dibenzoazepine residue is sizably bended (its two benzene rings forming an angle of 122°), a data consistent with the reported X-ray structure.⁷⁰ Moreover, the whole dibenzoazepine residue is almost perpendicular with respect to the perylene plane (80° of torsional angle). Derivative **5** calculated dipole moment is 5.98 Debye, lower than that of **3**, as expected due to the severe deviation from planarity. With the exclusion of derivative **4** (dipole moment 8.14 Debye), a purely D-A compound, all other molecules can be described as the combination of the donor-acceptor and twisted structures. In fact, all of them show a sizeable deviation from planarity (like in the case of *p*-terphenyl discussed in the Introduction and shown in Figure S1).

Table 1. Optimized HOMO and LUMO geometries (B3LYP/6-31G**), energies, torsional angle formed between perylene core and Donor residue and ground state dipole moment for derivatives **1-5** and **PMI-qs**.

PMI	HOMO (up) LUMO (down)	Torsional angle ($^\circ$)	μ (Debye)
1		61	5.93
2		62	4.75
3		45	6.70
4		-	8.14
5		80	5.98
PMI-qs		0	3.51

At the same time, the variation in the ground state molecular dipole moment as a function of the type of donor group (increasing in the order **2**<**1**<**5**<**3**<**4**) indicates the presence of a D-A behaviour (similar to that of DCM, figure S1).

65 Electrochemical, Spectroelectrochemical, UPS and Transient Absorption Characterizations.

The inspection of the differential pulse voltammetry (DPV) plots of a D-A compound family possessing the same acceptor and conjugated core enables to rank the donating capabilities of a donor series. In this study we used DPV instead of the more commonly employed cyclic voltammetry (CV) since some of our PMIs do not exhibit reversible oxidations (Figures 2a,b show the DPV plots. Figure S2 of the Supporting Information shows the

corresponding CV plots for all compounds). Donating substituents are expected to increase the electrochemically-derived HOMO energies according to their specific donating strength. Furthermore, if the donor and the acceptor ends are efficiently coupled, an increasing donating strength should also increase the LUMO energy as the accepting end, where most likely the LUMO is localized, becomes harder to reduce. Thus, when a particular donor mostly affects the HOMO energy without altering the LUMO, its coupling with the acceptor (and the extent of the π -conjugation) may be considered weak. The likely reasons for such behaviour are excessive bridge conjugation length and/or the presence of a sizeable torsional angle between the donor and the acceptor (the acceptor being, at least in our case, forced to be coplanar with the bridge). As such, the simultaneous inspection of both reduction and oxidation processes in a molecule series enables to rank the donor strength in terms of electron density effectively transferred towards the acceptor. It is worthwhile noting that DPV is not a direct vertical ionization technique, consequently, solvent stabilization of charged species as well as the reorganization energy always impact the electrochemically-derived HOMO and LUMO levels.⁶⁹ Thus, in parallel with electrochemical techniques we also employed ultraviolet photoemission spectroscopy (UPS) - a vertical ionization technique - and compared the results (Figure 2c-d). All DPV, UPS, and the resulting molecular orbital energies are collected in Table 2, along with corresponding calculated values.

Table 2. Comparison between the calculated, electrochemical and UPS estimates of the HOMO and LUMO levels for derivatives **1-5** and **PMI-qs**.

	1	2	3	4	5	PMI-qs
E_{pc}^{red} (V vs Fc^+/Fc)	-1.32	-1.29	-1.33	-1.41	-1.45	-1.84
E_{pc}^{ox} (V vs Fc^+/Fc)	0.25	0.79	0.52	0.29	0.36	-
Electrochemical HOMO (eV)	-5.48	-6.02	-5.75	-5.52	-5.59	-
Electrochemical LUMO (eV)	-3.65	-3.62	-3.66	-3.74	-3.78	-4.17
UPS HOMO (eV)	-5.20	-5.60	-5.45	-	-5.60	-5.95
Calculated HOMO	-5.09	-5.36	-5.17	-5.20	-5.47	-5.71
Calculated LUMO	-2.80	-2.88	-2.75	-2.64	-2.80	-3.18

DPV plots (Figures 2a,b) show that derivative **1**, the only compound exhibiting poor air stability, features the lowest oxidation potential in this series (+0.25 V vs Fc^+/Fc), with those of **2** (+0.79 V), **3** (+0.52 V), and **4** (+0.29 V) located at higher potentials. Thus, derivative **1** electrochemically-derived HOMO energy (-5.48 eV) is higher than those of derivatives **2-4** (**2**: -6.02 eV; **3**: -5.75 eV; **4**: -5.52 eV). Amongst the nitrogen based donors, the dibutylamine is the strongest one (derivative **4**) followed by the diphenylamine (derivative **3**) and next by the carbazole. Interestingly, the use of dibenzoazepine (derivative **5**), a supposedly very strong donor, leads to an electrochemical HOMO (-5.59 eV) intermediate between those of **3** and **4**. This result can be rationalized by the peculiar geometry of compound **5** (see previous paragraph). Dibutylamine remains the stronger

nitrogen-based donor as its nitrogen lone pair can be fully delocalized over the perylene bridge, not being shared by any other conjugated residue. The electrochemical LUMO levels (Table 2) show the same trend of the corresponding HOMOs, even though the differences in the corresponding energies are less pronounced, as expected by the calculated LUMOs, whose major contributions come from the perylene core.

We compared DPV results with solvent-independent UPS data. We included in the experiment the strongly electron-deficient derivative **PMI-qs**, which was previously used for luminescent solar concentrators. Figure 3c shows the high-binding energy cutoff region of the normalized photoemission spectra at -9V bias for compounds **1,2,3,5** and **PMI-qs**. The full photoemission spectra are reported in Figure S9 of the Supporting Information. The ionization potential of all solids is equal to the difference between the high-binding (low kinetic) cut-off energies and the low-binding (high-kinetic) Fermi edge onsets. Figure 2d shows the low-binding energy cutoff region highlighting the difference in the first ionization shoulder (*vide infra*).

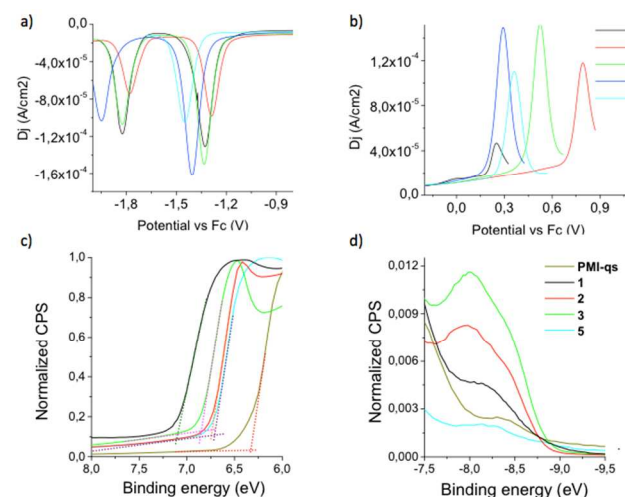


Figure 2. Electrochemical and UPS characterization of derivatives **1-5**. Reduction (a) and oxidation (b) DPV plots for derivatives **1-5** with tetrabutylammonium p-toluenesulfonate as the supporting electrolyte. c) Normalized photoemission spectra under a -9V bias for compounds **1,2,3,5** and the reference derivative **PMI-qs**. High-binding energy cutoff region. The onset for all of the spectra has been moved to -8.92 eV in order to evidence the arising difference in ionization potentials. d) Low-binding energy cutoff region highlighting the difference in the first ionization shoulder.

Table 2 shows the comparison between UPS ionization potentials and the corresponding calculated and electrochemical HOMO levels. The trend for derivatives **1, 2** and **3** is consistent with the DPV data. The deviations between the datasets possibly are ascribed to solvent/aggregation effects associated to the DPV experiments. However, in our case, the UPS and DPV datasets are almost superimposable for derivative **5**. Moreover, **5** and **2** UPS- and oxidation potential-derived HOMO energies are the same. Additionally, if we examine the low-binding energy region of the UPS spectra (Figure 2d) one can notice that while **1, 2** and **3** show a shoulder attributed to the first ionization process, both **PMI-Qs** and **5** show a weaker signal. While the lack of a peak is expected for **PDI-Qs** - an all acceptor compound - this result is unexpected for **5**. As observed previously for the naphthalene

analogue of **5**, the molecule is so severely twisted that D-A charge transfer becomes strongly impaired.⁷⁷ In the solid state derivatives **2** and **5** share the same deep HOMO level (-5.60 eV), closer to that of the all-acceptor derivative **PMI-qs** (-5.95 eV).

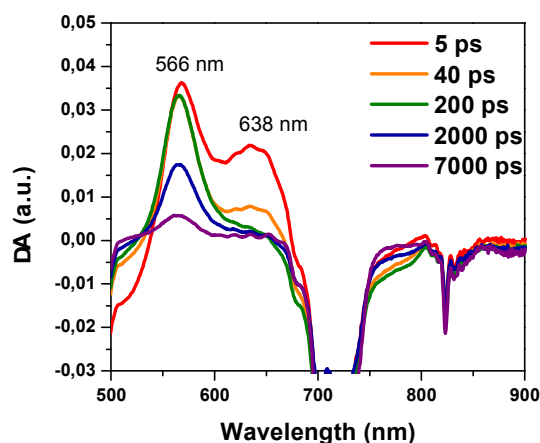


Figure 3. Differential transient absorption spectra of **5** (1.5×10^{-5} M) for 7 to 7000 ps after laser pulse irradiation at 480 nm in deaerated dichloromethane at 298 K.

Conversely, the DPV data place derivative **5** HOMO energy well above those of derivatives **2** and **3**. This inconsistency questions the real charge transfer nature of the HOMO-LUMO transition of derivative **5**. Indeed the inspection of the orbital densities of **5** in the gas phase suggests a marginal role of the donor group in both the ground and the first excited state electron densities (Table 1). Such conflicting data can be explained by taking into account a likely different geometry of **5** in solution with respect to both the solid state and the gas phases. However, to better characterize the nature of the HOMO-LUMO transition of **5** in solution, we carried out time-resolved transient absorption experiments in deaerated dichloromethane at room temperature and we compared the results with a spectroelectrochemical analysis in the same solvent.

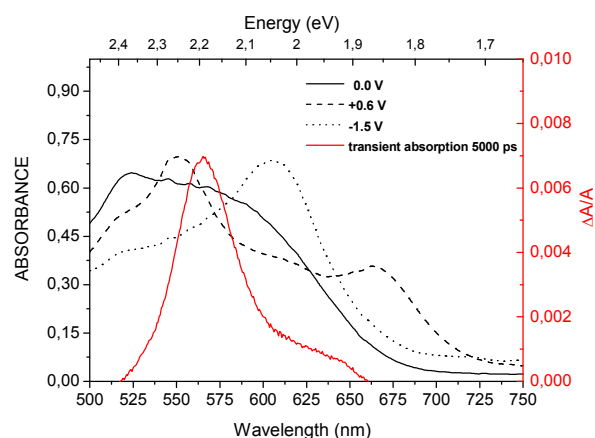


Figure 4. Comparison between the transient absorption spectrum at 5000 ps of a dichloromethane solution of **5** and the corresponding spectroelectrochemical absorption spectra of a CH_3CN solution of the same compound at no applied bias (solid line), -1.5 V (dotted line) and +0.6 V (dashed line). Potentials are reported versus the Fc/Fc^+ redox couple.

The transient spectra of **5** in the 500-700 nm region show intense absorption bands at 566 and 638 nm (Figure 3). Bleaches (negative ΔA) at $\lambda < 520$ nm and $\lambda > 700$ nm are due to ground state depletion and stimulated emission, respectively. The decay time of the absorption bands at 566 and 638 nm is in the order of a few nanoseconds. The absorption band at 638 nm decays with a first-order rate constant of $3.7 \times 10^{10} \text{ s}^{-1}$ (Figure 4a), while the change in the absorption at 566 nm occurs in two steps with first-order rate constants of $3.7 \times 10^{10} \text{ s}^{-1}$ and $2.3 \times 10^8 \text{ s}^{-1}$ (see Figures S11 and S12 of the Supporting Information). The initial fast process may be attributed to a conformational change of (**5**)^{*}, (e.g. increased planarity and $\text{sp}^3 \rightarrow \text{pseudo-sp}^2$ geometry of the linking dibenzoazepine nitrogen).⁷⁸ A direct excitation of the dibenzoazepine moiety and the consequent energy transfer from (PMI-1dibenzoazepine^{*}) to (1PMI^{*}-dibenzoazepine) should be excluded because the dibenzoazepine moiety does not absorb in the 480 nm region (i.e. excitation wavelength). Afterwards the signal decays according to a charge-transfer process from the dibenzoazepine donor to the PMI acceptor, in agreement with a D-A behaviour. These spectra correspond to the sum of the reduced (radical anion) and oxidized (radical cation) forms of **5** as obtained by a spectroelectrochemical experiment (Figure 4). The rate constant of the charge transfer process ($2.3 \times 10^8 \text{ s}^{-1}$; 4.3 ns) is consistent with the fluorescence lifetime of analogous PMI derivatives (~3 ns).⁷⁹

Multinuclear NMR investigation

Multinuclear ^1H and ^{13}C NMR spectroscopies can be of further aid in characterizing the effective electron donating capabilities of our donors. In fact, the inspection of the chemical shift of selected positions across the perylene bridge provides qualitative information about the amount of charge that a given donor is conveying towards the acceptor.

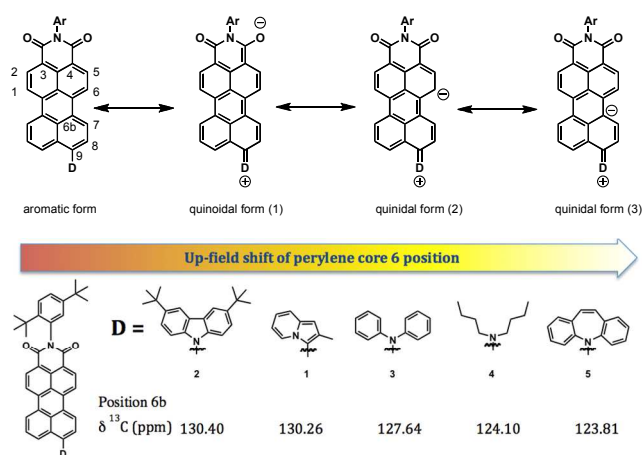


Figure 5. Top: canonical representations of a general PMI highlighting delocalization of donor charge on positions 6 and 6b. Bottom: ranking of the donating capabilities of different donors according to the ^{13}C chemical shift of carbon 6b.

This effect is distinct from and complementary to the HOMO energy increase evidenced by electrochemical and UPS techniques. NMR will monitor an increase in the charge transfer character through the chemical shift variations of the perylene core. We considered particularly meaningful the positions 6 and

6b, highlighted in the quinoidal forms (2) and (3) of the top part of Figure 5. In fact, according to the relative contribution of the aromatic versus quinoidal canonical description of the PMI ground state, the selected positions will show an upfield shift proportional to the donating strength of the employed donor.^{69,80,81}

Table S1 of the Supporting Information summarizes the ¹H and ¹³C NMR data for the positions 5,6,7,8 and 6b of the perylene core for **1-5**. The detailed inspection of all the data show the same trend, more or less pronounced, for all positions: an upfield shift of the ¹H and ¹³C NMR signals in the order **2**<**1**<**3**<**4**<**5**. We will discuss in particular the data referring to the ¹³C signals of positions 6b. This particular carbon is quaternary and unaffected by through-space effects. Moreover, as it is shown in the quinoidal form (3) of Figure 5, in one of the canonical representations of the general structure of our PMIs the charge residing on the Donor can be delocalized in that position. Thus, the ¹³C signal of position 6b for derivative **2** (130.40 ppm) is essentially the same as that of the corresponding signal for derivative **1** (130.26 ppm). This result reflects the inefficiency of indolizine to act as a π Donor, even though such residue is strongly electron rich (and thus easily oxidized) in electrochemical terms. Derivative **3** signal (127.64 ppm) is sizably upfield shifted, according to the documented donating capabilities of aromatic amines. Derivative **4** is even more upfield shifted (124.10 ppm). Exactly as in the case of the electrochemical ranking of donating capability, the NMR data confirm that an alkyl amine is a stronger donor with respect to an aryl one.⁶⁹ Finally, derivative **5** signal experiences the highest upfield shift in the series (123.81 ppm) confirming that, at least in solution, the dibenzoazepine residue is a stronger donor with respect to a standard aromatic amine and a comparable one with respect to aliphatic amines. The inspection of both ¹H and ¹³C signals of positions 6 and 8 shows the same trend, with the only exception of position 8 of derivative **4**, sizably upfield shifted with respect to the other compounds in the series. The deviation can be associated with the fact that this derivative is the only one featuring an alkyl substituent and thus unaffected by through space shielding effects that are instead affecting the position 8 of all other compounds.

UV-Vis absorption and emission spectroscopy.

Figure 5 shows the absorption (left) and emission (right) spectra of **1-5** in CHCl₃ and Table 4 summarizes all UV-Vis characterization data. Literature data shows that D-A PMIs are characterized by a broad and featureless absorption band peaking at 500-650 nm, sizeable Stokes shifts (3000-4000 cm⁻¹) and generally low emission efficiencies (< 40%).^{53,64}

This holds true for derivatives **3** and **4**, with **4** outperforming **3** in terms of Stokes Shift by 750 cm⁻¹. The absorption spectrum of **5** is also broad but with a distinguishable vibronic structure. The latter feature is connected with a less pronounced charge transfer behavior with respect to both **3** and **4**, as corroborated by the smaller Stokes shift (2560 cm⁻¹). In contrast to all other PMI, derivative **2** possesses a vibrationally structured absorption and a broad and featureless emission. Also, its Stokes shift (3790 cm⁻¹) is nearly as large as that of **4** (3814 cm⁻¹), even though carbazole hardly qualifies as a strong donor. Likewise, **2** is the only derivative in the series behaving mostly as a TW derivative with

very little D-A character. Upon optical excitation, this molecule undergoes a quinoidal distortion enforcing molecular planarity. The resulting major difference between the ground and first excited electronic states is responsible for the particularly large Stokes shift.

Table 3. UV-Vis molar extinction coefficients, absorption and emission maxima, luminescence quantum yields and Stokes shifts for derivatives **1-5** in toluene and CHCl₃ solutions. Luminescence quantum yields in PMMA slabs. Derivative **1** was not embedded in PMMA slabs for stability reasons.

Compound	λ_{max} Abs (nm)	λ_{max} Fluo (nm)	ϕ	ϵ (L mol ⁻¹ cm ⁻¹)	Stokes Shift (cm ⁻¹)
1 (CHCl ₃)	502	541	< 5 %	25600	1436
2 (toluene)	513	578	99 %	32000	2192
2 (CHCl ₃)	517	643	43 %	33000	3790
2 (PMMA) ^a			93 %		
3 (toluene)	550	629	95 %	31500	2284
3 (CHCl ₃)	560	676	56 %	31000	3064
3 (PMMA) ^a			73 %		
4 (toluene)	530	654	39 %	28000	3577
4 (CHCl ₃)	550	696	33 %	29000	3814
4 (PMMA) ^a			40 %		
5 (toluene)	562	646	73 %	30000	2314
5 (CHCl ₃)	577	677	36 %	29000	2560
5 (PMMA) ^a			70 %		

^a Absorption maxima of the slabs are not reported as the LSC demonstrators were too absorptive for UV-Vis spectrometers. Emission maxima depend on the distance with respect to the excitation point (see next section).

Derivatives **1** and **2** exhibit similar torsional angles; with the notable difference that indolizine in **1** is a stronger donor. This has profound consequences in terms of optical properties and photostability. The close inspection of derivative **1** absorption spectrum shows that its band is made of two contributions, a high energy absorbing, vibrationally structured one peaking at 504 nm and a low energy absorbing shoulder around 570 nm. The Stokes shift is unusually small (1436 cm⁻¹).

Also, the vibrationally resolved component of both the absorption and the emission bands of **1** closely resembles that of the unsubstituted (Donor = H) PMI **7** (see structure in Scheme S1). Interestingly, Figure S8 of the Supporting Information shows that upon exposure to direct sunlight in an air-equilibrated solution, the spectrum of **1** becomes superimposable to that of **7**. We believe that the low energy component of derivative **1** absorption corresponds to a through-space photoinduced charge transfer from the indolizine residue to the PMI core with consequent formation of an air-unstable indolizine radical cation and a PMI radical anion. While the anion can be reversibly quenched by molecular oxygen, the radical cation undergoes irreversible degradation.⁸² Such mechanism is likely to apply for all electron-rich and strongly twisted substituent. Figure S13 shows a cartoon highlighting the tentative mechanism for the observed degradation.

Analysis of the emission efficiencies is also particularly meaningful. First of all, derivative **4** is the only compound whose (low) emission efficiency does not change appreciably on going

from toluene to chloroform solutions. This is essentially a D-A chromophore and thus it exhibits low emission efficiency (39% and 33% in toluene and CHCl_3 respectively) and a large Stokes Shift. For all other compounds the emission efficiency is significantly higher in toluene (99, 95 and 73% for derivatives **2**, **3** and **5** respectively) than in chloroform (43, 56 and 36% for **2**, **3** and **5** respectively).

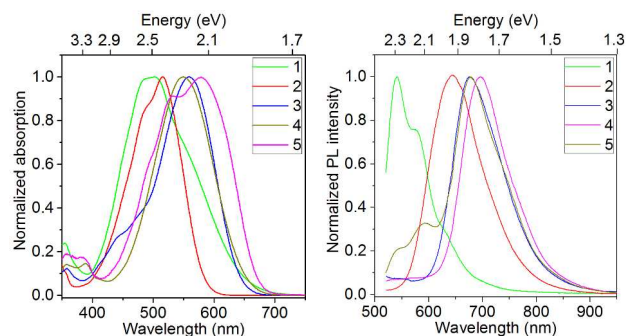


Figure 6. Normalized absorption (left) and emission (right) spectra of derivatives **1-5** in CHCl_3

Indeed, solvent polarity influences the interplay between D-A and TW regimes, as a polar solvent (chloroform) will enhance the former contribution, while a low polarity one (toluene) will do the opposite. Coherently, for all compounds possessing sizeable torsional angles (see Table 1) between the donor and the acceptor, low polarity solvents leads to higher luminescence quantum yields. For the purpose of the proposed application, the data in PMMA are particularly meaningful. In this case the emission efficiency will depend on polarity, as in the case of solutions, but also on viscosity. In fact, molecules possessing two conjugated fragments connected by a single bond having restricted rotational freedom, frequently behave as “molecular rotors”. The most distinctive characteristic of such class of compounds is an increase of the luminescence quantum yield upon increase of the local viscosity.⁶⁰ In particular, we recently introduced the naphthalene analogue of derivative **5** as a very efficient molecular rotor capable to probe the nanostructure of core-shell nanoparticles obtained through the self-assembly of amphiphilic block copolymers.⁷⁷

Indeed, with the sole exception of derivative **4** (a further confirmation of the purely Donor-Acceptor nature of this compound) all emission quantum yields in PMMA are systematically higher than the values in chloroform and generally comparable with those in toluene, even though the polarity of PMMA is even higher than that of chloroform. The value is particularly high for derivative **2**, again not surprisingly, as this is almost a purely twisted compound and thus a molecular rotor. As derivative **2** combines a very high Stokes Shift and the higher quantum yield in the series, we tested its performances as the luminophore in a LSC prototype.

Luminescent Solar Concentrator Devices.

A 10^{-4} M solution in PMMA/MMA syrup of the derivative **2** was heated in a cell cast immersed in a water bath at 56°C for 48 h. The cell cast was then annealed at 100°C for 12 h (see Supporting Information). During the whole process the sample remained homogeneous, without showing any sign of precipitation/phase

segregation. The slab was characterized in terms of the solid state quantum yield and re-absorption losses as a function of the distance between the excitation point and the slab edge where emitted light was collected. It is worthwhile to note that derivative **2** in PMMA matrix is almost as efficient (93%) as the reference Lumogen f 240 orange dye (perylene-3,4,9,11-tetracarboxylic acid bis-(2',6'-diisopropylanilide), quantum yield 99%).⁶⁸

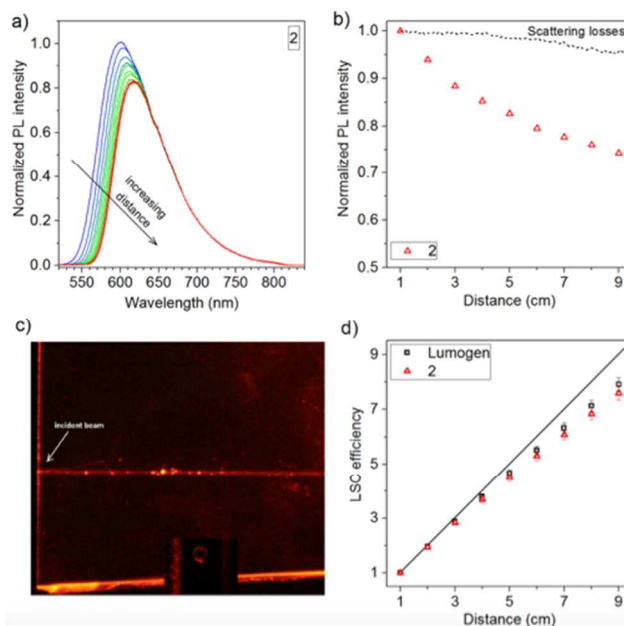


Figure 7. a) PL spectra excited at 405 nm at increasing distance (from 1 to 10 cm) between the excitation spot and detection at LSC edge for derivative **2**; b) Integrated PL output signal as a function of the distance from the excitation spot for derivatives **2**. For comparison also the scattering losses, obtained from the diffusion of a laser beam at 820 nm travelling through a pure PMMA slab (c), is reported. d) Total PL output for a linear growth of the slab size for a LSC based on the derivative **2** and for a reference LSC based on Lumogen f 240. The black-line indicates the “hypothetic” PL output increase for an ideal lossless sample.

Several processes including light scattering at the interfaces or inside the slab itself, and photoluminescence re-absorption affect the LSC efficiency. In order to isolate the optical losses due to the re-absorption, strictly related to the active dye efficiency, we plotted the evolution of the normalized emission spectrum as a function of the distance between the detection at the LSC edge and the excitation spot (laser operating @ 405 nm). The normalization was carried out on the low-energy tail of the spectrum ($\lambda > 730$ nm) where the re-absorption is negligible (Figure 7a). The PL spectrum shifts towards lower energies when increasing the distance, but the overall intensity is only slightly attenuated as clearly shown in Figure 7b. Thus, for an optical path of 10 cm the LSC based on the derivative **2** retains about 80% of its initial intensity. Figure 7b also reports the scattering losses obtained from the attenuation of a laser @ 820 nm (photon energy below the band gap) traveling through the slab (figure 7c). The scattering contribution is generally very small and constant throughout the sample, additional evidence that any further improvement of LSC performances will mostly depend on the optimization of the luminophore properties in terms of Stokes shift and luminescence quantum yield.

Conclusions

Our findings demonstrate that derivative **2** represents an optimal trade off as it shows both a very large Stokes shift and a high emission quantum yield. This compound represents a significant entry in the field of luminescent materials for LSC and is a valid alternative to the traditional Lumogen dyes for the fabrication of larger area devices. Indeed, Figure 7d compares the estimated total PL output as a function of the LSC size for slabs doped with derivative **2** and with Lumogen f 240 orange. As expected, the tendency of the total emitted light to saturate by increasing the device dimensions is rather small for both LSC devices, whose performances are indistinguishable within the experimental uncertainty even though derivative **2** luminescence quantum yield is sizably smaller. The use of the latter is in any case advantageous as its red shifted emission spectrum corresponds to the region of maximum External Quantum Yield of silicon solar cells.

Notes and references

^a Department of Materials Science, Università di Milano-Bicocca, via Cozzi 55, 20125, Milano, Italy E-mail: luca.beverina@unimib.it

^b Polyera Corporation, 8045 Lamon Avenue, Suite 140, Skokie, IL 60077.

^c Department of Chemistry and the Argonne-Northwestern Solar Energy Research Center, Northwestern University, Evanston, Illinois, 60208 USA

† Electronic Supplementary Information (ESI) available: Synthetic procedures for the preparation of derivatives **1-4**. Copy of the ¹H and ¹³C NMR for all new compounds. Details on computational investigation. Details on electrochemical, UPS and time resolved emission characterizations. Details on PMMA samples preparation. Details on the photodegradation of derivative **1**. See DOI: 10.1039/b000000x/ Authors gratefully acknowledge the financial support of “Fondazione Cariplo” through grant 2010-0564 “Luminescent Solar Concentrators for Building Integrated Photovoltaics – LumiPhoto”.

- C. Huang, S. Barlow, and S. R. Marder, *J. Org. Chem.*, 2011, **76**, 2386–2407.
- F. Würthner and M. Stolte, *Chem. Commun.*, 2011, **47**, 5109–5115.
- X. Zhan, A. Facchetti, S. Barlow, T. J. Marks, M. A. Ratner, M. R. Wasielewski, and S. R. Marder, *Adv. Mater.*, 2011, **23**, 268–284.
- C. Liu, C. Xiao, Y. Li, W. Hu, Z. Li, and Z. Wang, *Chem. Commun.*, 2014, **50**, 12462–12464.
- T. Weil, T. Vosch, J. Hofkens, K. Peneva, and K. Müllen, *Angew. Chem. Int. Ed.*, 2010, **49**, 9068–9093.
- L. Ferlauto, F. Liscio, E. Orgiu, N. Masciocchi, A. Guagliardi, F. Biscarini, P. Samori, and S. Milita, *Adv. Funct. Mater.*, 2014, **24**, 5503–5510.
- K. Trofymchuk, A. Reisch, I. Shulov, Y. Mély, and A. S. Klymchenko, *Nanoscale*, 2014, **6**, 12934–12942.
- R. C. Savage, E. Orgiu, J. M. Mativetsky, W. Pisula, T. Schnitzler, C. L. Eversloh, C. Li, K. Müllen, and P. Samori, *Nanoscale*, 2012, **4**, 2387.
- G. Griffini, L. Brambilla, M. Levi, M. Del Zoppo, and S. Turri, *Sol. Energy Mater. Sol. Cells*, 2013, **111**, 41–48.
- J. E. Anthony, A. Facchetti, M. Heeney, S. R. Marder, and X. Zhan, *Adv. Mater.*, 2010, **22**, 3876–3892.
- L. Cerdán, A. Costela, G. Durán-Sampedro, I. García-Moreno, M. Calle, M. Juan-y-Seva, J. de Abajo, and G. A. Turnbull, *J. Mater. Chem.*, 2012, **22**, 8938–8947.
- P.-O. Schwartz, L. Biniek, E. Zaborova, B. Heinrich, M. Brinkmann, N. Leclerc, and S. Méry, *J. Am. Chem. Soc.*, 2014, **136**, 5981–5992.
- J. M. Mativetsky, M. Kastler, R. C. Savage, D. Gentilini, M. Palma, W. Pisula, K. Müllen, and P. Samori, *Adv. Funct. Mater.*, 2009, **19**, 2486–2494.
- Z. Liu, C. Tonnelé, G. Battagliarin, C. Li, R. A. Gropeanu, T. Weil, M. Surin, D. Beljonne, R. Lazzaroni, M. Debliquy, J.-M. Renoirt, and K. Müllen, *J. Phys. Chem. B*, 2014, **118**, 309–314.
- D. Görl, X. Zhang, and F. Würthner, *Angew. Chem. Int. Ed.*, 2012, **51**, 6328–6348.
- A. Sarbu, L. Biniek, J.-M. Guenet, P. J. Mésini, and M. Brinkmann, *Journal of Materials Chemistry C*, 2015, **3**, 1235–1242.
- T. Ribeiro, S. Raja, A. S. Rodrigues, F. Fernandes, C. Baleizão, and J. P. S. Farinha, *Dyes and pigments*, 2014, **110**, 227–234.
- S. Fery-Forgues, *Nanoscale*, 2013, **5**, 8428.
- M. M. Sartin, C. Huang, A. S. Marshall, N. Makarov, S. Barlow, S. R. Marder, and J. W. Perry, *J. Phys. Chem. A*, 2014, **118**, 110–121.
- Z. An, S. A. Odom, R. F. Kelley, C. Huang, X. Zhang, S. Barlow, L. A. Padilha, J. Fu, S. Webster, D. J. Hagan, E. W. Van Stryland, M. R. Wasielewski, and S. R. Marder, *J. Phys. Chem. A*, 2009, **113**, 5585–5593.
- X. Huang, Q. Shi, W.-Q. Chen, C. Zhu, W. Zhou, Z. Zhao, X.-M. Duan, and X. Zhan, *Macromolecules*, 2010, **43**, 9620–9626.
- J. Fortage, M. Séverac, C. Houamer-Rassin, Y. Pellegrin, E. Blart, and F. Odobel, *J. Photoch. Photobio. A*, 2008, **197**, 156–169.
- C. Li, A. Keerthi, Z. Liu, Y. Liu, J. Schöneboom, Q. Wang, F. Eickemeyer, S. Valiyaveetil, N. G. Pschirer, P. Erk, A. Herrmann, and K. Müllen, *J. Mater. Chem.*, 2009, **19**, 5405–5415.
- T. Edvinsson, T. Edvinsson, C. Li, C. Li, N. Pschirer, N. Pschirer, J. Schöneboom, J. Schöneboom, F. Eickemeyer, F. Eickemeyer, R. Sens, R. Sens, G. Boschloo, G. Boschloo, A. Herrmann, A. Herrmann, K. Mullen, K. Mullen, A. Hagfeldt, and A. Hagfeldt, *J. Phys. Chem. C*, 2007, **111**, 15137–15140.
- L. Le Pleux, A. L. Smeigh, E. Gibson, Y. Pellegrin, E. Blart, G. Boschloo, A. Hagfeldt, L. Hammarström, and F. Odobel, *Energy Environ. Sci.*, 2011, **4**, 2075.
- E. Kozma and M. Catellani, *Dyes and pigments*, 2013, **98**, 160–179.
- C. Li and H. Wonneberger, *Adv. Mater.*, 2012, **24**, 613–636.
- M. G. Debijs and P. P. C. Verbunt, *Adv. Energy Mater.*, 2012, **2**, 12–35.
- W. G. J. H. M. van Sark, K. W. J. Barnham, L. H. Slooff, A. J. Chatten, A. Büchtemann, A. Meyer, S. J. McCormack, R. Koole, D. J. Farrell, R. Bose, E. E. Bende, A. R. Burgers, T. Budel, J. Quilitz, M. Kennedy, T. Meyer, C. D. M. Donegá, A. Meijerink, and D. Vanmaekelbergh, *Opt. Express*, 2008, **16**, 21773–21792.
- B. Rowan, L. Wilson, and B. Richards, *IEEE J. Quantum. Elect.*, 2008, **14**, 1312–1322.
- H. Hernandez-Noyola, D. Potterveld, R. Holt, and S. B. Darling, *Energy Environ. Sci.*, 2012, **5**, 5798–5802.
- L. Beverina and A. Sanguineti, *Solar Cell Nanotechnology*, 2013, 317–356.
- V. Fattori, M. Melucci, L. Ferrante, M. Zambianchi, I. Manet, W. Oberhauser, G. Giambastiani, M. Frediani, G. Giachi, and N. Camaioni, *Energy Environ. Sci.*, 2011, **4**, 2849–2853.
- M. Melucci, M. Durso, L. Favaretto, M. L. Capobianco, V. Benfenati, A. Sagnella, G. Ruani, M. Muccini, R. Zamboni, V. Fattori, and N. Camaioni, *RSC Adv.*, 2012, **2**, 8610–8613.
- J. C. Goldschmidt, M. Peters, A. Bösch, H. Helmers, F. Dimroth, S. W. Glunz, and G. Willeke, *Sol. Energy Mater. Sol. Cells*, 2009, **93**, 176–182.
- M. J. Currie, J. K. Mapel, T. D. Heidel, S. Goffri, and M. A. Baldo, *Science*, 2008, **321**, 226–228.
- N. D. Boscher, P. Choquet, D. Duday, N. Kerbellec, J.-C. Lambrechts, and R. Maurau, *J. Mater. Chem.*, 2011, **21**, 18959–18961.
- R. H. Inman, G. V. Shcherbatyuk, D. Medvedko, A. Gopinathan, and S. Ghosh, *Opt. Express*, 2011, **19**, 24308–24313.
- V. M. Agranovich, Y. N. Gartstein, and M. Litinskaya, *Chem. Rev.*, 2011, **111**, 5179–5214.
- L. Slooff, E. Bende, A. Burgers, T. Budel, M. Pravettoni, R. Kenny, E. Dunlop, and A. Büchtemann, *physica status solidi (RRL)-Rapid Research Letters*, 2008, **2**, 257–259.

41. C. L. Mulder, L. Theogarajan, M. Currie, J. K. Mapel, M. A. Baldo, M. Vaughn, P. Willard, B. D. Bruce, M. W. Moss, C. E. McLain, and J. Morseman, *Adv. Mater.*, 2009, **21**, 3181–3185.
42. S. F. H. Correia, V. de Zea Bermudez, S. J. L. Ribeiro, P. S. André, R. A. S. Ferreira, and L. D. Carlos, *J. Mater. Chem. A*, 2014, **2**, 5580–5596.
43. A. Sanguineti, A. Monguzzi, G. Vaccaro, F. Meinardi, E. Ronchi, M. Moret, U. Cosentino, G. Moro, R. Simonutti, M. Mauri, R. Tubino, and L. Beverina, *Phys Chem Chem Phys*, 2012, **14**, 6445–6448.
44. J. Graffion, A. M. Cojocariu, X. Cattoën, R. A. S. Ferreira, V. R. Fernandes, P. S. André, L. D. Carlos, M. W. C. Man, and J. R. Bartlett, *J. Mater. Chem.*, 2012, **22**, 13279–13285.
45. C. Freund, W. Porzio, U. Giovannella, F. Vignali, M. Pasini, S. Destri, A. Mech, S. Di Pietro, L. Di Bari, and P. Mineo, *Inorg. Chem.*, 2011, **50**, 5417–5429.
46. X. Wang, T. Wang, X. Tian, L. Wang, W. Wu, Y. Luo, and Q. Zhang, *Sol. Energy*, 2011, **85**, 2179–2184.
47. O. Moudam, B. C. Rowan, M. Alamiry, P. Richardson, B. S. Richards, A. C. Jones, and N. Robertson, *Chem. Commun.*, 2009, 6649.
48. C. S. Erickson, L. R. Bradshaw, S. McDowall, J. D. Gilbertson, D. R. Gamelin, and D. L. Patrick, *ACS Nano*, 2014, **8**, 3461–3467.
49. F. Meinardi, A. Colombo, K. A. Velizhanin, R. Simonutti, M. Lorenzon, L. Beverina, R. Viswanatha, V. I. Klimov, and S. Brovelli, *Nature Photon*, 2014, **8**, 392–399.
50. F. Purcell-Milton and Y. K. Gun'ko, *J. Mater. Chem.*, 2012, **22**, 16687–16697.
51. W. E. Benjamin, D. R. Veit, M. J. Perkins, E. Bain, K. Scharnhorst, S. McDowall, D. L. Patrick, and J. D. Gilbertson, *Chem. Mater.*, 2014, **26**, 1291–1293.
52. C. Haines, M. Chen, and K. P. Ghiggino, *Sol Energ Mat Sol C*, 2012, **105**, 287–292.
53. P. D. Zoon and A. M. Brouwer, *Photochem. Photobiol. Sci.*, 2009, **8**, 345–353.
54. G. Brusatin, P. Innocenzi, A. Abbotto, L. Beverina, G. A. Pagani, M. Casalbani, F. Sarcinelli, and R. Pizzoferrato, *Journal of the European Ceramic Society*, 2004, **24**, 1853–1856.
55. P. V. Bernhardt, R. Koch, D. W. J. Moloney, M. Shtaiwi, and C. Wentrup, *J. Chem. Soc., Perkin Trans. 2*, 2002, **0**, 515–523.
56. S. R. Marder, L. T. Cheng, B. G. Tiemann, A. C. Friedli, M. Blanchard-Desce, J. W. Perry, and J. Skindhoj, *Science*, 1994, **263**, 511–514.
57. X. Feng, P. Wu, F. Bolze, H. Leung, K. Li, N. Mak, D. Kwong, J. Nicoud, K. Cheah, and M. Wong, *Org. Lett.*, 2010, **12**, 2194–2197.
58. P. Salice, S. Versari, S. Bradamante, F. Meinardi, G. Macchi, G. A. Pagani, and L. Beverina, *Organic Photonics and Photovoltaics*, 2013, **2013**, 39–55.
59. I. López-Duarte, T. T. Vu, M. A. Izquierdo, J. A. Bull, and M. K. Kuimova, *Chem. Commun.*, 2014, **50**, 5282–5284.
60. N. Amdursky, Y. Erez, and D. Huppert, *Accounts Chem. Res.*, 2012, **45**, 1548–1557.
61. E. J. Alexy, J. M. Yuen, V. Chandrashaker, J. R. Diers, C. Kirmaier, D. F. Bocian, D. Holten, and J. S. Lindsey, *Chem. Commun.*, 2014, **50**, 14512–14515.
62. Y. Zagranyski, L. Chen, Y. Zhao, H. Wonneberger, C. Li, and K. Müllen, *Org. Lett.*, 2012, **14**, 5444–5447.
63. C. Jiao, K.-W. Huang, C. Chi, and J. Wu, *J. Org. Chem.*, 2011, **76**, 661–664.
64. C. Li, J. Schöneboom, Z. Liu, N. G. Pschirer, P. Erk, A. Herrmann, and K. Müllen, *Chem. Eur. J.*, 2009, **15**, 878–884.
65. P. D. Zoon and A. M. Brouwer, *Chemphyschem*, 2005, **6**, 1574–1580.
66. N. Tasios, C. Grigoriadis, M. R. Hansen, H. Wonneberger, C. Li, H. W. Spiess, K. Müllen, and G. Floudas, *J. Am. Chem. Soc.*, 2010, **132**, 7478–7487.
67. H. Langhals and A. Hofer, *J. Org. Chem.*, 2012, **77**, 9585–9592.
68. A. Sanguineti, M. Sassi, R. Turrisi, R. Ruffo, G. Vaccaro, F. Meinardi, and L. Beverina, *Chem. Commun.*, 2013, **49**, 1618–1620.
69. O. Kwon, S. Barlow, S. A. Odom, L. Beverina, N. J. Thompson, E. Zojer, J.-L. Brédas, and S. R. Marder, *J Phys Chem A*, 2005, **109**, 9346–9352.
70. M. T. Reetz, S. H. tte, R. Goddard, and U. Minet, *J. Chem. Soc., Chem. Commun.*, 1995, 275–277.
71. H. Langhals, G. Schonmann, and L. Feiler, *Tetrahedron Letters*, 1995, **36**, 6423–6424.
72. Y. Nagao, Y. Abe, and T. Misono, *Dyes and pigments*, 1991, **16**, 19–25.
73. A. Facchetti, L. Vaccaro, and A. Marrocchi, *Angew. Chem. Int. Ed.*, 2012, **51**, 3520–3523.
74. B. Ligault, D. Lapointe, L. Caron, A. Vlassova, and K. Fagnou, *J. Org. Chem.*, 2009, **74**, 1826–1834.
75. S. B. Darling, *J. Phys. Chem. B*, 2008, **112**, 8891–8895.
76. Y. Shao, L. F. Molnar, Y. Jung, J. Kussmann, C. Ochsenfeld, S. T. Brown, A. T. B. Gilbert, L. V. Slipchenko, S. V. Levchenko, D. P. O'Neill, R. A. DiStasio, R. C. Lochan, T. Wang, G. J. O. Beran, N. A. Besley, J. M. Herbert, C. Y. Lin, T. Van Voorhis, S. H. Chien, A. Sodt, R. P. Steele, V. A. Rassolov, P. E. Maslen, P. P. Korambath, R. D. Adamson, B. Austin, J. Baker, E. F. C. Byrd, H. Dachsel, R. J. Doerksen, A. Dreuw, B. D. Dunietz, A. D. Dutoi, T. R. Furlani, S. R. Gwaltney, A. Heyden, S. Hirata, C.-P. Hsu, G. Kedziora, R. Z. Khalliulin, P. Klunzinger, A. M. Lee, M. S. Lee, W. Liang, I. Lotan, N. Nair, B. Peters, E. I. Proynov, P. A. Pieniazek, Y. M. Rhee, J. Ritchie, E. Rosta, C. D. Sherrill, A. C. Simmonett, J. E. Subotnik, H. L. Woodcock, W. Zhang, A. T. Bell, A. K. Chakraborty, D. M. Chipman, F. J. Keil, A. Warshel, W. J. Hehre, H. F. Schaefer, J. Kong, A. I. Krylov, P. M. W. Gill, and M. Head-Gordon, *Physical Chemistry Chemical Physics*, 2006, **8**, 3172–3191.
77. G. Vaccaro, A. Bianchi, M. Mauri, S. Bonetti, F. Meinardi, A. Sanguineti, R. Simonutti, and L. Beverina, *Chem. Commun.*, 2013, **49**, 8474–8476.
78. M. Iwamura, S. Takeuchi, and T. Tahara, *J. Am. Chem. Soc.*, 2007, **129**, 5248–5256.
79. S. E. Miller, Y. Zhao, R. Schaller, V. Mulloni, E. M. Just, R. C. Johnson, and M. R. Wasielewski, *Chem. Phys.*, 2002, **275**, 167–183.
80. L. M. Tolbert and M. E. Ogle, *J. Am. Chem. Soc.*, 1990, **112**, 9519–9527.
81. A. Abbotto, S. Bradamante, and G. A. Pagani, *J. Org. Chem.*, 2001, **66**, 8883–8892.
82. H. Ko, S. Kim, W. Choi, B. Moon, and H. Lee, *Chem. Commun.*, 2005, 69–71.